Cyclic regulation of Trpm4 expression in female vomeronasal neurons driven by ovarian sex hormones

Eugenia Eckstein[a,1], Martina Pyrski[a,1], Silvia Pinto[b], Marc Freichel[c], Rudi Vennekens[b], Frank Zufall[a,*]

[a] Center for Integrative Physiology and Molecular Medicine, Saarland University, Homburg, Germany
[b] Laboratory of Ion Channel Research, TRP Research Platform Leuven (TRPLe), Department of Cellular and Molecular Medicine, KU Leuven, Leuven, Belgium
[c] Institute of Pharmacology, University of Heidelberg, Heidelberg, Germany

ARTICLE INFO

ABSTRACT

The vomeronasal organ (VNO), the sensory organ of the mammalian accessory olfactory system, mediates the activation of sexually dimorphic reproductive behavioral and endocrine responses in males and females. It is unclear how sexually dimorphic and state-dependent responses are generated by vomeronasal sensory neurons (VSNs). Here, we report the expression of the transient receptor potential (TRP) channel Trpm4, a Ca^{2+}-activated monovalent cation channel, as a second TRP channel present in mouse VSNs, in addition to the diacylglycerol-sensitive Trpc2 channel. The expression of Trpm4 in the mouse VNO is sexually dimorphic and, in females, is tightly linked to their reproductive cycle. We show that Trpm4 protein expression is upregulated specifically during proestrus and estrus, when female mice are about to ovulate and become sexually active and receptive. The cyclic regulation of Trpm4 expression in female VSNs depends on ovarian sex hormones and is abolished by surgical removal of the ovaries (OVX). Trpm4 upregulation can be restored in OVX mice by systemic treatment with 17ß-estradiol, requires endogenous activity of aromatase enzyme, and is strongly reduced during late pregnancy. This cyclic regulation of Trpm4 offers a neural mechanism by which female mice could regulate the relative strength of sensory signals in their VSNs, depending on hormonal state. Trpm4 is likely to participate in sex-specific, estrous cycle-dependent and sex hormone-regulated functions of the VNO, and may serve as a previously unknown genetic substrate for dissecting mammalian sexually dimorphic cellular and behavioral responses.

1. Introduction

The transient receptor potential (TRP) channel Trpm4, a member of the TRPM subfamily, is a Ca^{2+}-activated monovalent cation channel that is regulated by several factors including temperature, phosphatidylinositol-4,5-bisphosphate (PIP$_2$), and ATP (Launay et al., 2002; Murakami et al., 2003; Nilius et al., 2003; Liman, 2007; Mathar et al., 2014). Trpm4 allows Na$^+$ entry into the cells upon activation, but it is impermeable to Ca^{2+}. Trpm4 functions in immune cells where it regulates Ca^{2+} oscillations after T cell activation (Launay et al., 2004) and Ca^{2+} entry in mast cells (Vennekens et al., 2007). Trpm4 contributes also to cardiovascular physiology and pathophysiology (Mathar et al.,

2014). More recently, Trpm4 has been implicated in sweet, bitter, and umami signaling of taste receptor cells of the tongue (Dutta Banik et al., 2018). The function of Trpm4 in the nervous system remains incompletely understood, although a number of studies indicated a role for Trpm4 in excitotoxicity, axonal degeneration, and neuronal cell death (Schattling et al., 2012; Simard et al., 2012; Leiva-Salcedo et al., 2017; Simard and Gerzanich, 2018). Thus, gaining a detailed understanding of the role of Trpm4 in nerve cells remains an important goal.

The vomeronasal organ (VNO) is the chemosensory organ of the mammalian accessory olfactory system (Brennan and Zufall, 2006; Tirindelli et al., 2009; Chamero et al., 2012; Liberles, 2014; Mohrhardt et al., 2018), housing ~300,000 vomeronasal sensory neurons (VSNs)

in the mouse (Leinders-Zufall et al., 2009). These neurons mediate the detection of pheromones (Leinders-Zufall et al., 2000; Chamero et al., 2007; Haga et al., 2010) and other socially relevant chemosignals including predator odors (Papes et al., 2010; Pérez-Gómez et al., 2015) and illness-associated cues (Boillat et al., 2015; Bufe et al., 2019), and thus orchestrate a wide variety of social behaviors. VSNs respond to chemostimulation with a receptor-operated, G protein-coupled intracellular signaling cascade leading to the opening of the TRP channel Trpc2 (for a recent review, see Mohrhardt et al., 2018). Trpc2 is a Ca^{2+}-permeable cation channel that is activated by diacylglycerol (DAG) and inhibited by intracellular Ca^{2+}-calmodulin (Lucas et al., 2003; Spehr et al., 2009; Leinders-Zufall et al., 2018). The development of photoswitchable DAGs revealed that millisecond DAG pulses are sufficient to activate Trpc2 (Leinders-Zufall et al., 2018). Genetic disruption of inositol 1,4,5-trisphosphate (InsP$_3$) signaling showed no obvious effect on VSN primary chemoelectrical signal transduction (Chamero et al., 2017).

Whether additional TRP channels besides Trpc2 could contribute to VSN signaling has been a long-standing question (Zufall, 2014). Two previous studies have identified Ca^{2+}-activated nonselective (CAN) cation channels in VSNs of hamster (Liman, 2003) and mouse (Spehr et al., 2009), but there is so far no candidate TRP protein shown to be expressed in these cells. On the basis of their functional properties, it has been suggested that the CAN currents of hamster VSNs are likely encoded by *Trpm4* (Liman, 2007). Several other results suggest that additional cation channels could contribute to VSN excitation. Cellular responses to some VSN stimuli remained unaffected in Trpc2-deficient mice (Kelliher et al., 2006; Trouillet et al., 2019), and a pheromonal recognition memory was evoked through vomeronasal sensing in a Trpc2-independent manner (Kelliher et al., 2006). Furthermore, VSN responses seem to exhibit much more flexibility and plasticity than initially anticipated (Brennan and Zufall, 2006; Dey et al., 2015; Xu et al., 2016; Marom et al., 2019) suggesting the existence of yet unknown modulatory mechanisms in VSNs. Particularly interesting in this context is the result that VSN signaling can be temporarily silenced through the female sex-steroid progesterone (Dey et al., 2015). These results together with other findings highlight the fact that pheromone responses can vary across the female ovulation cycle and are sexually dimorphic and state-dependent (Stowers and Liberles, 2016; Yang and Shah, 2016), and that sex and gonadal steroids generally play important roles in mammalian pheromonal communication and sexually dimorphic behaviors (Baum and Bakker, 2013; Yang and Shah, 2014).

Here we report the discovery of Trpm4 as a second TRP channel expressed in VSNs. We find that Trpm4 expression is synchronized to the female reproductive cycle. This cyclic regulation of Trpm4 is governed by ovarian sex hormones, specifically 17ß-estradiol. Therefore, hormone-regulated Trpm4 expression in the VNO provides a previously unknown molecular substrate for future dissection of sexually dimorphic responses underlying mammalian pheromonal communication.

2. Materials & methods

2.1. Experimental model and subject details

All animal protocols and experimental procedures complied with the ethical guidelines for the care and use of laboratory animals established by the German Animal Welfare Act, European Communities Council Directive 2010/63/EU, and the institutional ethical and animal welfare guidelines of Saarland University School of Medicine (approval number H-2.2.4.1.1). Mice (6–12 weeks, both sexes) were kept with food and water *ad libitum* in micro-isolator cages under a 12:12-hour light/dark cycle. Animals are regularly tested for pathogens by diagnostic screening of sentinel mice using serology and PCR. Surgical manipulation of mice was performed in a class IIA laminar flow biosafety cabinet. Generation of the Trpm4-IRES-Cre knockin mice

(Trpm4-IC) is described below. These mice were crossed with a ROSA26 reporter strain (eR26-tauGFP; Gt(ROSA)26Sor$^{tm1(CAG-Mapt/GFP)Uboe}$ (Wen et al., 2011; Kusumakshi et al., 2015; Pyrski et al., 2017). The resulting offspring were heterozygous for both Cre recombinase and τGFP. Colabeling experiments also used heterozygous OMP-GFP mice (B6; 129P2-Omp$^{tm3Mom/MomJ}$, The Jackson Laboratory, stock #006667) in which all cells expressing olfactory marker protein (OMP) are labeled by green fluorescent protein (GFP) (Potter et al., 2001). A mouse strain carrying a global Trpm4 knockout mutation ($Trpm4^{-/-}$, Trpm4$^{tm1.1Mfre}$) (Vennekens et al., 2007) served as control for the specificity of Trpm4 immunoreactivity (IR). For developmental experiments, we used C57BL/6N (denoted as B6) mice of both sexes (Charles River, Sulzfeld, Germany) at different ages from postnatal day 1 (P1), P7, P14, to P21. Ovariectomy and hormone replacement experiments were conducted on female B6 mice at 8 and 9 weeks of age, respectively. Time-pregnant females (Charles River, Sulzfeld, Germany) were 8–10 weeks of age. According to the animal welfare suggestions, we have minimized the number of mice where possible to reach a minimum of at least 3 subjects per experimental group for statistical purpose.
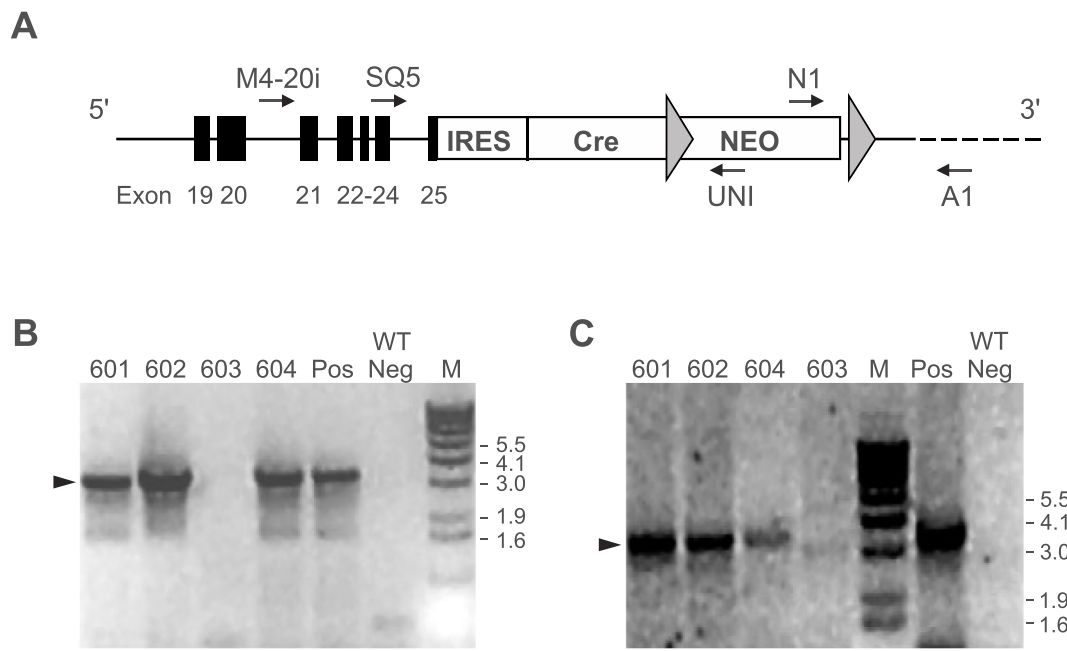
2.2. Generation of Trpm4-IRES-Cre mice

Using standard cloning techniques, we created an IRES-Cre-Frt Neo Frt construct which was inserted after the STOP codon of the Trpm4 gene using homologous recombination in BA1 (C57Bl/6N × 129/SVeV) hybrid embryonic stem cells. Targeted stem cells were microinjected into C57BL/6 blastocysts. Resulting chimeras with a high percentage agouti coat color were mated to C57BL/6N mice to generate F1 heterozygous offspring. Tail DNA was analyzed from pups with agouti or black coat color. The presence of the IRES-Cre-Frt Neo Frt cassette was amplified with primers SQ5 and UNI. SQ5 is located on the long homology arm, upstream of the introduced cassette. UNI is located inside the Neo cassette (Fig. 1). Homologous recombination was demonstrated by PCR amplification using primers located inside the positive selection cassette and outside the homologous arms (N1/A1 resulting in a 3.5 kb fragment for the 3′ arm, and M4-20i/UNI resulting in a 3.2 kb fragment for the 5′ arm) and sequencing of the amplification products. Tail DNA samples from mice with the targeted allele were amplified with primers N1 and A1. Apart from the screening of offspring, all steps were performed by InGenious Targeting Laboratory (Ronkonkoma, NY 11779, USA). F1 offspring was crossed with Flp-recombinase expressing mice (The Jackson Laboratory, USA) to remove the Neomycin (NEO) selection gene. Deletion of the NEO cassette was confirmed by tail genomic PCR using primers N1 and A1. Further offspring was standardly genotyped and used for breeding.

Primers used for PCR-based genotyping (5′-3′ orientation) were SQ5: TGCTTGTGTGACAGGCACTTTG; UNI: AGCGCATCGCCTTCTATC GCCTTC; N1: TGCGAGGCCAGAGGCCACTTGTGTAGC; A1: CTGACTCT GCAAGGATCTCTAGAG; M4-20i: CGCATTTATTCCCTATTTGTGC.

2.3. Immunohistochemistry

Mice were anesthetized with a mixture of 165 mg/kg bodyweight ketamine (Pharmacia GmbH, Berlin, Germany) and 11 mg/kg bodyweight xylazine (Bayer Health Care, Leverkusen, Germany), and transcardially perfused with phosphate-buffered saline (PBS), pH 7.4, followed by 2% (*w/v*) paraformaldehyde in PBS. VNOs were dissected, postfixed for 2 h in 2% paraformaldehyde in PBS and equilibrated for at least 48 h in 30% sucrose solution in PBS. The tissue was embedded in OCT (Tissue-Tek) and frozen in a dry ice/2-methylbutane bath. Tissue sections of 12 μm were cut, collected on glass slides (Superfrost Plus, Polysciences), and stored at −80 °C until subjected to immunohistochemical analyses. All immunohistochemical procedures were performed at room temperature, if not otherwise noted. Sections were rinsed in PBS, incubated in blocking solution containing 0.3%

Fig. 1. Generation of Trpm4-IRES-Cre mice. (A) Schematic representation of the targeting strategy to create a Trpm4-IRES-Cre mouse. An IRES-Cre cassette is introduced in the 3' UTR, after the *Trpm4* STOP codon located in exon 25. The neomycin (NEO) cassette is flanked by Frt sites (grey triangles) and was removed through Flp mediated recombination. Primer locations and orientations are indicated by black arrows. (B) PCR screening for introduction of the cassette, using primers SQ5 and UNI and tail genomic DNA from F1 generation mice. Offspring from chimeric mice 601, 602 and 604 are positive for integration (arrowhead), and were used for further breeding. (C) PCR screening of the F1 offspring from chimeric mice 601, 602 and 604 using primers N1 and A1 confirmed integration of the short homology arm in the genome (arrowhead). M, DNA size standard in kilo base pairs is as indicated.

Triton X-100 and 4% normal horse serum (Vector Laboratories) in PBS for 1 h, followed by incubation in blocking solution containing primary antibody for at least overnight at 4 °C. Primary antibodies were: Trmp4 (1:100; rabbit polyclonal, Alomone Labs, cat# ACC-044, Lot#AN02; RRID: AB_2040250), Trpc2 (1:2000, rabbit polyclonal) (Liman et al., 1999) kindly provided by P. Mombaerts (Max Planck Research Unit for Neurogenetics, Frankfurt, Germany), OMP (1:1000, goat polyclonal, Wako cat# 544-10001-WAKO, RRID: AB_664696) and GFP (1:1000, chicken polyclonal, Abcam, cat# ab13970, RRID:AB_300798). Tissue sections were washed three times 10 min in PBS and incubated in secondary antibody solution for 1 h in the dark. Secondary antibodies were: Alexa Fluor 488 goat anti-rabbit (1:1000, Thermo Fisher Scientific, cat# A-11034, RRID:AB_2576217), Alexa Fluor 488 goat anti-chicken (Thermo Fisher Scientific, cat# A-11039, RRID:AB_2534096), and Alexa Fluor 555 donkey anti-rabbit (1:1000, Thermo Fisher Scientific, cat# A-31572, RRID:AB_162543). Tissue sections were rinsed in PBS, the nuclei counterstained with Hoechst 33342 (1:10000, Invitrogen) for 10 min, and cover slipped using fluorescence mounting medium (DAKO). For double-labeling experiments of Trpm4 and Trpc2, a rabbit block was included to prevent cross-reactivity of the antibodies. Therefore, after the first immunohistochemistry, tissue sections were incubated for 1 h in blocking solution containing 2% normal rabbit serum. After a short rinse in PBS, sections were incubated for 1 h in goat anti-rabbit Fab-fragments diluted in PBS (1:50; BioMol, Rockland, cat# 811-7102, RRID:AB_218909). Sections were washed 3 times for 10 min in PBS, incubated in second primary antibody over night at 4 °C, followed by incubation in fluorescence-conjugated secondary antibody and Hoechst nuclear stain.

2.4. Fluorescence microscopy

Fluorescence images were taken with a BX61 epifluorescence microscope attached to a DP71 camera (Olympus) and a LSM 880/ ConfoCor-3 confocal microscope (Zeiss) using the appropriate excitation and emission barrier filters. Acquired digital images were minimally adjusted for brightness and contrast using Photoshop Elements 10 (Adobe Photoshop).

2.5. RNA extraction and cDNA synthesis

Total RNA of VNO was obtained from 8 to 12 weeks old B6 mice and extracted using the innuPREP RNA mini kit (Analytik Jena) following the manufacturer's protocol. RNA integrity and concentration was assessed by gel electrophoresis and spectrophotometry (Ultraspec 2100 pro, Amersham Biosciences) using a spectrosil, 5 mm, super sub micro cuvette (Amersham Biosciences). Total RNA from 7 to 10 pooled VSNs of Trpm4-IC/eR26-τGFP mice was extracted after dissociation and microscopic selection of individual cells. Tissue dissociation and manual collection of single cells was as described (Pyrski et al., 2017). VNO epithelium of 8 to 12 weeks old Trpm4-IC/eR26-τGFP mice was stripped from the bone capsules and incubated for 20 min at 37 °C in dissociation buffer containing 0.22 units/ml papain (Worthington), 1.1 mM EDTA (Thermo Scientific), 5.5 mM L-cysteine hydrochloride (Sigma), diluted in 1 ml PBS. Cell suspensions were supplemented with 1 ml DNA digestion mixture (600 μl PBS, 400 μl Colorless GoTaq reaction buffer (Promega) and 50 units of DNase I (Thermo Scientific)), incubated for 5 min at RT and digestion was stopped by adding 10 ml DMEM (Invitrogen) supplemented with 10% (v/v) fetal calf serum (FCS). Following centrifugation (5 min at 1000 × g, 4 °C), olfactory cells were resuspended in 50 μl DMEM supplemented with 10% (v/v) FCS and seeded on glass coverslips coated with 0.5 mg/ml concanavalin A (Sigma) and incubated in 5% CO_2 at 37 °C for 1 h in a cell culture incubator. Individual τGFP+ cells were identified by fluorescence microscopy (BX50WI, Olympus), manually collected in glass capillaries, transferred to 3–5 μl S2 solution (145 mM NaCl, 5 mM KCl, 10 mM HEPES, 1 mM $MgCl_2$, 1 mM $CaCl_2$, 10 mM glucose), snap frozen in liquid nitrogen and stored at −80 °C until further use.

cDNA synthesis was as described (Pyrski et al., 2017). In brief, 0.5 μg of total RNA, 1.5 μl CDS primer (10 μM,

AGCAGTGGTAACAACGCAGAGTACTTTTTTTTTTTTTTTTTTTTTTTTTTT-TTTVN, Clontech) and 1.5 µl Smart II primer (10 µM, AAGCAGTGGT ATCAACGCAGAGT, Clontech) were adjusted to a total volume of 7.5 µl with DEPC-treated water and samples were incubated for 2 min at 65 °C and 2 min on ice. Subsequently, a reaction mix containing 1.5 µl dNTP mix (10 mM, Agilent Technologies), 0.5 µl RNase inhibitor (20 U/µl, Promega), 1.5 µl 10× AMV buffer (NEB) and 1.5 µl AMV reverse transcriptase (10 U/µl, NEB) was added to the reaction. cDNA was synthetized in intervals for 30 min at 42 °C, for 10 min at 45 °C, for 10 min at 50 °C, and for 10 min at 55 °C. Following heat inactivation of the enzyme (5 min at 65 °C), the volume of the cDNA solution was adjusted to 50 µl. For isolated cells, cDNA synthesis was performed as for the whole tissue samples, except that 3–5 µl S2 solution containing the cells was directly added to the cDNA reaction mixture and the final volume of the cDNA was adjusted to 20 µl.

2.6. RT-PCR and quantitative real time RT-PCR

RT-PCR was performed using 0.5 µl cDNA and the Phusion High Fidelity DNA polymerase (Thermo Scientific) according to the manufacturer's protocol. Gene-specific forward (F) and reverse (R) primers to amplify full-length *Trpm4* and *Trpm5* were (5′-3′ orientation): *Trpm4*-F (exon 1): GGCCGGAGAAGGAGCA, *Trpm4*-R (exon 25): GGATGCAAAC ACCTAGACATCCA (4,234 bp amplicon, https://www.ncbi.nlm.nih. gov/nuccore/NM_175130.4) and Trpm5-F (1. ATG): ATGCAAACAACC CAGAGCTCCT, *Trpm5*-R (exon 25): GAAGGTTGATGTGCCCCAAAAA (4,123 bp amplicon). As control for cellular identity, we used *Omp*-F: ATGGCAGAGGATGGGCC and *Omp*-R: GAGCTGGTTAAACACCACAGA GGC (489 bp amplicon). Amplification conditions included an initial denaturation for 15 s at 98 °C, followed by 39 cycles of (10 s at 98 °C–10 s at 60 °C–60 s (*Trpm4*, *Trpm5*) or 20 s (*Omp*) at 72 °C), and a final elongation (5 min at 72 °C). The specificity of PCR products was confirmed by direct DNA sequencing (Seqlab) of PCR-products.

Quantitative PCR for female B6 VNO at different estrous cycle stages (diestrus and estrus) was performed on a My-iQ-cycler (Bio-Rad) using iTaq™Universal SYBR® Green Supermix (Bio-Rad) according to the manufacturer's protocol. We conducted three independent experiments comprising VNO samples of 6 animals each group. Gene-specific forward and reverse primers were *Trpm4*-F (exon 22): TCGGGACAAGCG AGACAGTGA, *Trpm4*-R (exon 24): AGGCAGCAAGGCAGAGTGGCTAA and *Gapdh*-F: TGAACGGATTTGGCCGTATTGG, *Gapdh*-R: TGCCGTTGA ATTTGCCGTGAG. PCR conditions were an initial denaturation for 3 min at 95 °C, followed by 39 cycles of (30 s at 95 °C–20 s at 64 °C–30 s at 72 °C). Reactions were performed as triplicates on 96-well plates with each sample containing the VNO of two mice and analyzed with the iQ5 Software (Bio-Rad). Controls for RNA isolation, PCR conditions and the linearity of amplification were evaluated according to MIQE guidelines. The specificity of PCR products was confirmed by direct DNA sequencing (Seqlab). The copy number was calculated using a calibration curve for the primer set with a defined amount of copies as starting material, diluted in tRNA solution.

2.7. Estrous cycle assessment

Vaginal cytology was assayed by vaginal smear examination (Caligioni, 2009; Oboti et al., 2014; Blum et al., 2019). Vaginal smears were obtained daily at 09:00 h from mature virgin B6 female mice. Vaginal flushes using 20 µl of PBS were examined using a bright field microscope (Bresser, LCD Micro 5MP, Leica DM 750). Representative examples of vaginal smear histology across the mouse estrous cycle are shown below in Fig. 4A.

2.8. Surgical procedures and hormone replacement

Adult female B6 mice (8 weeks) were deeply anesthetized by intraperitoneal injection of 100 mg/kg body weight ketamine and 6 mg/

kg body weight xylazine and OVX was performed to ablate endogenous hormone production of ovaries. Analgesia was provided by administration of 5 mg/kg body weight Carprofen (Rimadyl, 50 mg/ml, Pfizer, Scotland). After a recovery period of at least 7 days, mice were randomly assigned to 5 hormonal treatment groups. Hormone reservoirs (ME2–30, MP4–30, Belma Technologies, Liège, Belgium) were implanted subcutaneously under short-term anesthesia. Implants are designed to release daily doses of hormone reaching physiological plasma concentrations of progesterone (~15 ng/ml) and 17ß-estradiol (~60 pg/ml pre-ovulatory concentration). Group 1 females ($n = 4$) served as controls and received vehicle implants, group 2 females ($n = 10$) received 17ß-estradiol implants (ME2–30, E2). After a period of 14 days, six females of group 2 were injected intraperitoneally with progesterone (4 µg/g bodyweight) dissolved in sesame oil and were perfused 6 h and 24 h after injection (groups 3 and 4). Group 5 females ($n = 4$) received progesterone implants (MP4–30, P4). Estrous cycle was monitored daily throughout the experiment (37 days) with intermissions during recovery periods. Mice were sacrificed 14 days after hormone implantation and VNO tissue was collected for immunohistochemical analyses.

2.9. Systemic aromatase inhibition

Endogenous production of estradiol in 8 weeks old B6 female mice ($n = 3$) was blocked by systemic administration of the aromatase inhibitor exemestane (6-methylideneandrosta-1,4-diene-3,17-dione) (Sigma-Aldrich, St. Louis, Missouri, US). Females received 5 mg/kg bodyweight exemestane ($n = 3$) or vehicle (5% DMSO in sesame oil; $n = 3$) by intraperitoneal injection once a day for 5 consecutive days. Estrous cycle was monitored daily throughout the experiment (19 days).

2.10. Cell counts and fluorescence quantification

Cell counts were performed manually on acquired epifluorescence images (Olympus BX61) of Trpm4-stained VNO sections counterstained with Hoechst 33342 nuclear dye (see 2.3.). Images were taken from sections of the anterior, middle and posterior VNO of mice at the different age stages (P7, P14, and P21), with 3–4 sections each from $n \geq 3$ mice. Images were acquired from the central part of the vomeronasal sensory epithelium (VNE) at 400× magnification using a region of interest (ROI) frame width of 218 µm. Camera live images were black-balanced using cellSense software (Olympus) to subtract background staining of the glass slide. Trpm4 staining of VSNs was then visually evaluated. Numbers of Trpm4 labeled VSNs were determined using the multipoint counting option of ImageJ software (NIH) and expressed as percentage of the number of counterstained nuclei set as 100% in each image. Cell counts from VNE sections were averaged for each mouse.

Trpm4 and Trpc2 immunofluorescence was quantified as mean fluorescence intensity (mean grey value in arbitrary units (a.u.) in the region of interest, ROI) of 12-bit confocal images (LSM 880, Zeiss) that were acquired as 0.8 µm and 6 µm thick optical sections, respectively. Confocal scanning parameters were kept the same for all tissue sections to allow comparison of mean fluorescent intensities even among different experiments. Images were taken from the anterior, middle and posterior VNO of mice. 3–8 VNO sections were acquired from each mouse and mean fluorescent intensities were measured. For Trpm4, we used the freehand selection tool of ImageJ to encircle the VNE in each image (ROIs of ~30,000 µm²). For Trpc2, a ROI of ~500 µm² (5 µm × 100 µm rectangle) was placed into the microvillous layer of the VNE.

2.11. Statistical analyses

Quantitative PCR data were examined with the software Origin Pro 2017G (OriginLab Corporation, Northampton, MA, USA). The

significance of difference between two distributions was measured using the unpaired Student's *t*-test. All quantitative PCR data are expressed as means ± SD. A value of $p \leq 0.05$ was considered as statistically significant. No data or subjects were excluded from this study. Statistical analyses on mean fluorescence intensity of immunoreactivity on tissue sections were performed using Origin Pro 2020 software. Multiple groups were compared using a one-way analysis of variance (ANOVA) with Tukey's *post hoc* test for comparison. If normal distribution failed, data were analyzed using Kruskal-Wallis ANOVA and Mann-Whitney *U post hoc* test. In all analyses, the probability of error level (alpha) was chosen to be 0.05. Data are expressed as means ± SD.

3. Results

3.1. Widespread expression of Trpm4 in VSNs of sexually naïve male and female mice

On the basis of physiological recordings in VSNs from hamster (Liman, 2003) and mouse (Spehr et al., 2009), we hypothesized that Trpm4 could represent a second TRP channel expressed in VSNs besides Trpc2. To assess Trpm4 expression in the VNO, we constructed a novel Trpm4-IRES-Cre knockin strain that enables mapping and characterization of *Trpm4*-expressing cells employing a binary genetic strategy (Fig. 1A-C). To monitor Cre recombinase activity, these mice were bred with a fluorescent ROSA26 reporter strain (Wen et al., 2011; Kusumakshi et al., 2015; Pyrski et al., 2017) to generate Trpm4-IC/eR26-τGFP double knockin mice. In these mice, τGFP reports the history of activity of the *Trpm4* promoter, thus labeling both cells that used to express Trpm4 as well as cells that acutely express Trpm4 at the time of analysis.

We conducted immunohistochemistry (IHC) for τGFP in coronal cryosections of the VNE from sexually naïve, adult male or female mice (7 weeks old) and observed that virtually all VSNs were positive for τGFP (τGFP+) (Fig. 2A). Strong τGFP immunoreactivity (IR) was also present in supporting cells and in the nonsensory epithelium of the VNO (Fig. 2A). To determine whether Cre-mediated τGFP expression reports acute Trpm4 protein expression in VSNs, we employed a knockout-validated polyclonal anti-Trpm4 antiserum that is directed against amino acid residues 5–17 of the *N*-terminus of human TRPM4. Double labeling IHC for Trpm4 and τGFP revealed Trpm4 protein expression (Trpm4+) in the vast majority of τGFP+ VSNs of both males and females (Fig. 2B). However, in 50% (3/6) of female mice Trpm4-IR appeared weak or perhaps absent in the VNE despite the presence of normal τGFP-IR (Fig. 2C).

Trpm4+ VSN somata and dendrites were found in all depths of the VNE with no zonal restrictions (Fig. 2B, D). There was no evidence for Trpm4-IR in VSN axons (Fig. 2D). Trpm4-IR in VNE from OMP-GFP mice (Potter et al., 2001) confirmed that labeled cells were indeed mature VSNs (Fig. 2D). The specificity of Trpm4-IR was verified by the lack of any signal in age-matched Trpm4 knockout ($Trpm4^{-/-}$) male mice (Vennekens et al., 2007) (Fig. 2E). We obtained independent support for these results by RT-PCR analyses of cDNA prepared from whole VNO tissue or from fluorescently-labeled, manually-collected VSNs (Pyrski et al., 2017) obtained from adult (7 weeks) Trpm4-IC/eR26-τGFP males or females and C57BL/6 (denoted as B6) mice (Fig. 2F). Using gene-specific primers flanking the complete coding region of *Trpm4* mRNA (exon 1 - exon 25), we obtained amplicons of the expected sizes of ~4 kb from both sexes (Fig. 2F). Sequence analyses confirmed that the PCR products correspond to the full-length *Trpm4* channel known to encode a functional Ca^{2+}-activated monovalent cation channel (Launay et al., 2002; Nilius et al., 2003). By contrast, mRNA for full-length *Trpm5*, which encodes a second Ca^{2+}-activated monovalent cation channel (Liman, 2007; Pyrski et al., 2017),
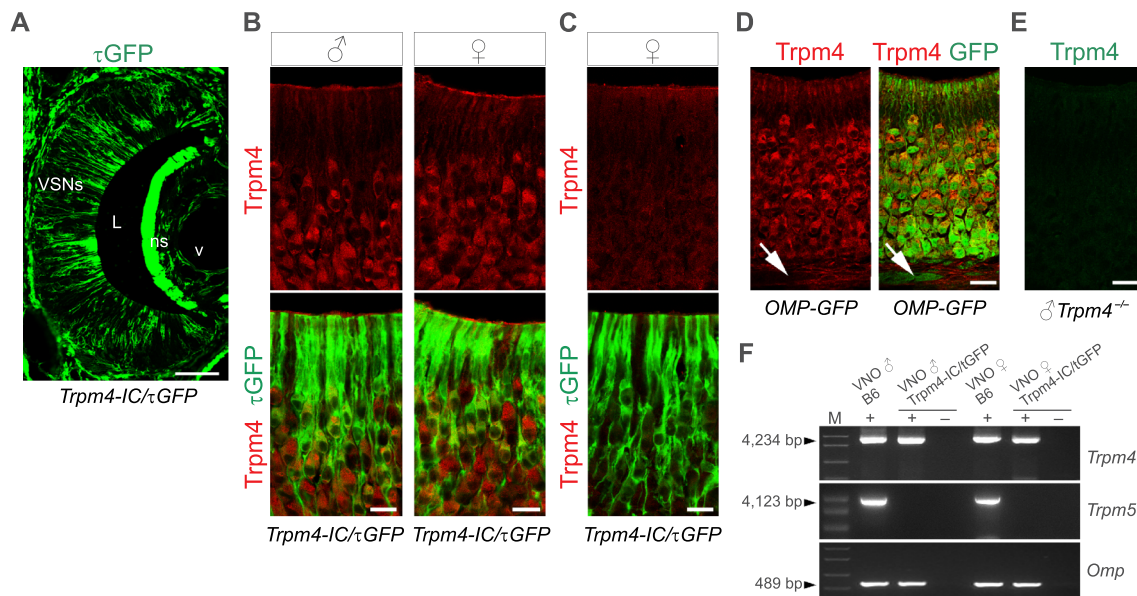
Fig. 2. Trpm4 is expressed in VSNs of sexually naïve male and female mice. (A) τGFP immunostaining (green) in a coronal cryosection of the left VNO of a 7-week-old Trpm4-IC/eR26-τGFP mouse reports widespread Trpm4 gene expression in sensory neurons and in supporting cells of the VNE. τGFP-IR is also present in cells of the non-sensory (ns) epithelium and in vascular endothelial cells. (B) Magnification of the VNE of male (♂) and female (♀) Trpm4-τGFP reporter mice show that Trpm4 protein (red) colocalizes with τGFP fluorescence (green) in VSNs but is absent in supporting cells. (C) In about 50% of females, VSNs were devoid of Trpm4 protein despite the presence of τGFP. (D) The vast majority of Trpm4+ VSNs (red) colocalizes with the olfactory marker protein (OMP, green), a marker for mature VSNs, in somata, dendrites and dendritic knobs, but not in VSN axon bundles (arrows). (E) The specificity of the Trpm4 antibody is verified by the absence of immunoreactivity in the VNO of $Trpm4^{-/-}$ male mice. (F) RT-PCR analysis of *Trpm4* and *Trpm5* mRNA prepared from whole VNO and from isolated VSNs (7–10 cells/sample) of male and female B6 and Trpm4-IC/eR26-τGFP mice. Sequence analysis confirmed that the 4.2 kb *Trpm4* amplicon (arrowhead) in each sample encodes full-length *Trpm4* mRNA. The 4.1 kb *Trpm5* amplicon (arrowhead) encoding the full-length *Trpm5* mRNA was only detected in whole VNO but absent in isolated VSNs. Identity of dissociated VSNs was verified by RT-PCR for olfactory marker protein (*Omp*). Control reactions omitting reverse transcriptase (−RT) showed no PCR products ruling out genomic DNA contamination. Scale bars (A) 200 μm, (B-E) 20 μm.
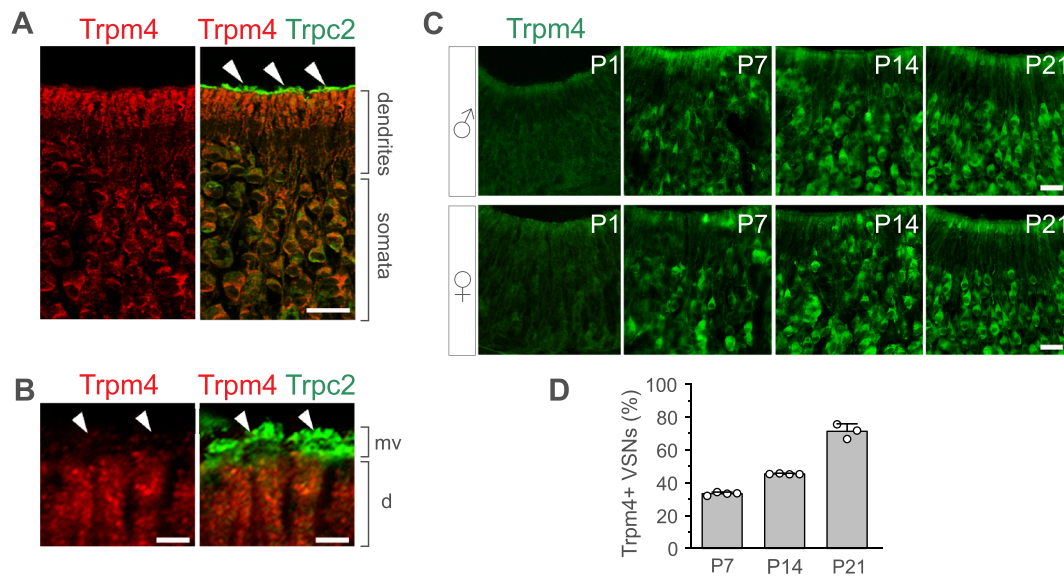
Fig. 3. Trpc2 but not Trpm4 protein localizes to VSN microvilli. (A) Double labeling of Trpm4 (red) and Trpc2 (green) depicts co-localization of both TRP channels in VSN somata and dendrites (right panel). The most apical layer (arrowheads) shows robust Trpc2 labeling (green). (B) High-resolution confocal image (1-μm optical section) of the dendritic endings (d) of VSNs shows that microvilli (mv) are heavily labeled for Trpc2 (green, arrowheads) whereas Trpm4-IR (red) was not detected in the microvilli. (C) Representative examples of Trpm4-IR (green) in coronal sections of VNE from B6 mice at postnatal days (P) 1, P7, P14 and P21. Trpm4 protein expression emerges at around P7. Number of Trpm4 + VSNs increases with age. (D) Quantification of Trpm4 + VSNs over developmental time as percentages of the total number of VSNs determined by nuclear Hoechst staining: P7 (33 ± 1%, $n = 2$ male and 2 female mice, 13 sections, 3–4 sections/mouse); P14 (45 ± 0.2%, $n = 2$ male and 2 female mice, 15 sections, 3–4 sections/mouse); P21 (71 ± 4.5%, $n = 1$ male and 2 female mice, 12 sections, 4 sections/mouse). Individual data points represent the averaged cell counts obtained from a single mouse. Data are expressed as means ± SD. Scale bars (A, B) 20 μm, (C) 2 μm.

was absent from these identified VSNs but present in whole VNO tissue (Fig. 2F), consistent with its role in solitary chemosensory cells of the VNO (Ogura et al., 2010; Tizzano et al., 2011).

To assess the subcellular distribution of Trpm4 in VSN compartments in more detail, we conducted double labeling IHC for Trpm4 and Trpc2, the principal transduction channel of VSNs (Liman et al., 1999; Leypold et al., 2002; Stowers et al., 2002; Lucas et al., 2003). We found that Trpm4 protein is abundantly expressed in VSN dendritic knobs, dendrites and somata but, unlike Trpc2, is not detectable in VSN microvilli which represent the primary signal transduction compartment (Fig. 3A, B). We therefore conclude that Trpm4 does not function in VSN microvilli, but instead occupies a cellular location that is in close proximity to the major Ca^{2+} store organelles, endoplasmic reticulum and mitochondria in the dendritic knob and dendrite.

We also investigated Trpm4-IR in the VNE at different developmental time points between birth and weaning using VNO sections derived from male and female B6 mice at postnatal days P1, P7, P14, and P21 (Fig. 3C, D). Irrespective of sex, we found that Trpm4 expression in VSNs emerges around P7 with an increasing number of Trpm4 + cells towards adulthood (Fig. 3C). Trpm4-IR was virtually absent at P1 ($n = 2$ male and 2 female mice). At P7 33% (1082/3254 VSNs, $n = 2$ male and 2 female mice), at P14 45% (1638/3636 VSNs, $n = 2$ male and 2 female mice), and at P21 71% (1742/2464, $n = 1$ male and 2 female mice) of VSNs were Trpm4 + (Fig. 3D). Thus, Trpm4 protein expression in VSNs begins a few days after birth and reaches a maximum at adulthood.

Collectively, these results identify Trpm4, in addition to Trpc2, as a second major TRP channel expressed in mouse VSNs. However, unlike Trpc2, Trpm4 is not detectable in the microvilli of VSNs. This spatial location suggests that Trpm4 does not mediate primary VSN signal transduction, but rather would be an ideal candidate for downstream or modulatory functions in VSNs. These results are fully consistent with previous recordings of a Trpm4-like channel at the dendritic tips of mouse VSNs (Spehr et al., 2009) and a similar channel found in hamster VSNs (Liman, 2003).

3.2. Vomeronasal Trpm4 expression is sexually dimorphic and depends on the female estrous cycle

Next, we systematically investigated Trpm4 expression in adult female mice and compared the results with those obtained in males (Fig. 4). Adult females undergo distinct hormonal changes during their estrous cycle, which has a length of 4–5 days in mice and is characterized by four different stages: metestrus, diestrus, proestrus, and estrus (Levine, 2015). We assayed vaginal cytology to identify the estrous stage (Fig. 4A) and then performed Trpm4-IR (Fig. 4B). These experiments revealed a surprising cyclic regulation of Trpm4 expression in female VSNs: Trpm4-IR was low or abolished in females residing at the post-ovulatory phase (metestrus and diestrus) whereas a robust increase in Trpm4-IR was observed during the pre-ovulatory phase (proestrus and estrus) (Fig. 4B, H). To verify the specificity of this effect, we performed control experiments in $Trpm4^{-/-}$ females at estrus; there was no vomeronasal Trpm4-IR in these mice despite exhibiting a normal estrous cycle (Fig. 4C). For comparison, we also examined expression of Trpc2 but observed no cyclic regulation of Trpc2-IR in female VNE (Fig. 4E, I). VSNs from adult males did not exhibit differences in Trpm4 expression and showed equally abundant Trpm4-IR among the males investigated ($n = 6$; Fig. 4D; see also Fig. 2).

To gain some insight into the molecular basis underlying Trpm4 cyclic regulation in females, we performed quantitative real time RT-PCR (qPCR) analyses during the reproductive cycle. We analyzed total RNA samples from VNOs of B6 mice using gene-specific primers for *Trpm4* and quantified *Trpm4* mRNA levels at two different cycle stages, diestrus and estrus (Fig. 4F). Three independent experiments using 6 mice in each group revealed approximately two-fold higher *Trpm4* mRNA levels during estrus (144 ± 33 copies/ng total RNA) *versus* diestrus (77 ± 24 copies/ng total RNA; $p < 0.05$). Thus, cyclic expression of Trmp4 in the female VNO may be regulated at the mRNA level. Consistent with these results, quantification of Trpm4 immunofluorescence showed 2 to 3-fold increases in mean grey values during proestrus and estrus as compared to the levels observed at metestrus and diestrus (Fig. 4H).
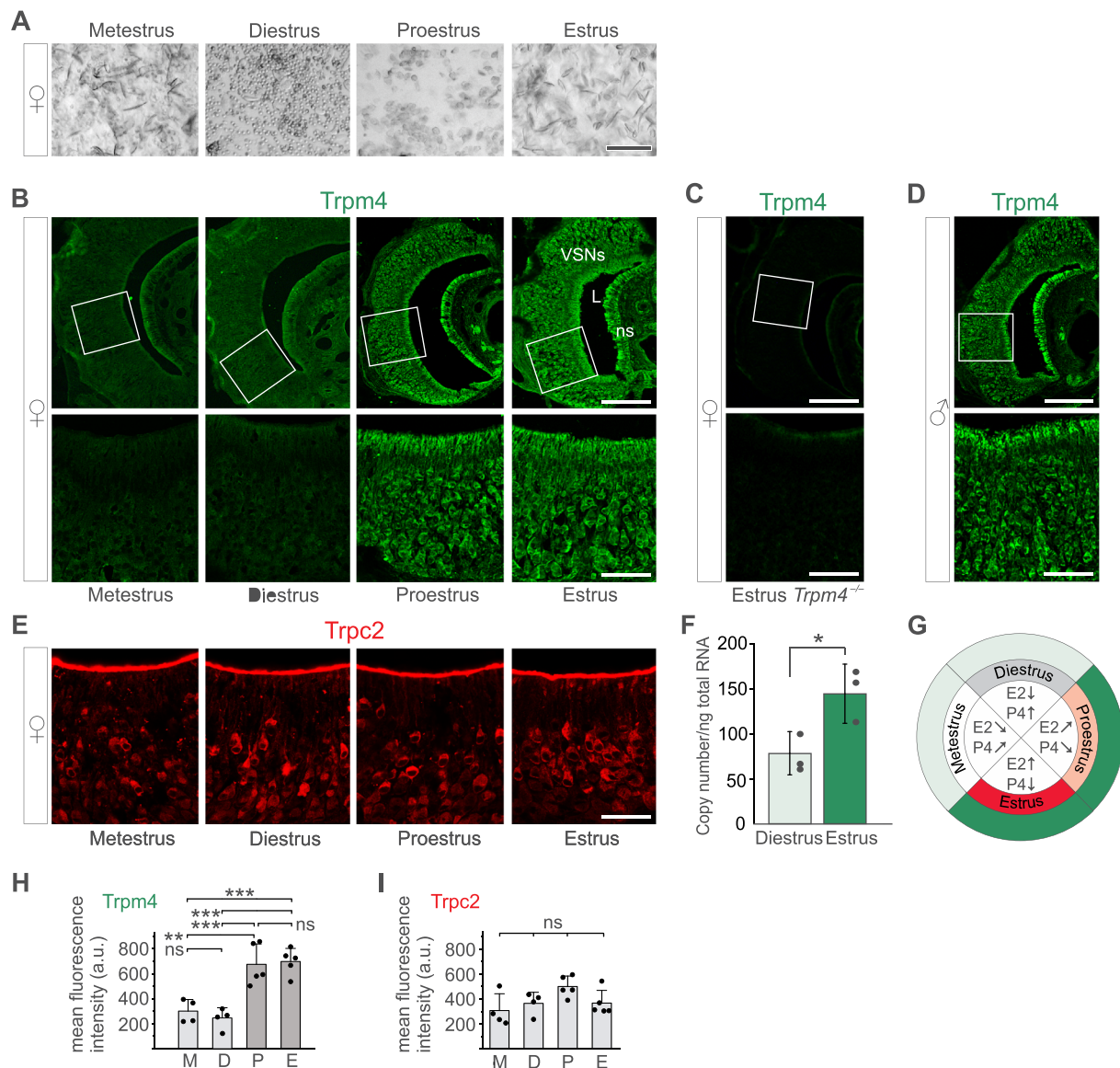
Fig. 4. Sexually dimorphic and estrous cycle-dependent expression of Trpm4 in VSNs.

(A) Representative bright field images illustrating the cellular composition of vaginal fluid during the four estrous cycle stages metestrus (leucocytes, nucleated and cornified epithelial cells), diestrus (leucocytes), proestrus (nucleated epithelial cells) and estrus (cornified epithelial cells). (B) Trpm4-IR (green) in coronal sections of the female (♀) VNO during the estrous cycle (n = 3 female VNOs/stage). Trpm4-IR is pronounced in VSNs during proestrus and estrus but close to detection threshold during metestrus and diestrus. (C) The specificity of the Trpm4 antiserum is verified by the lack of any Trpm4-IR in VNO of $Trpm4^{-/-}$ female mice at estrus. (D) Representative IHC for Trpm4 (green) in a coronal section of a male (♂) VNO exemplifying the persistent Trpm4 expression in VSNs among the mice investigated (n = 6 males). (E) Trpc2-IR (red) in coronal sections of female VNOs isolated at different stages of the estrous cycle showing that Trpc2 expression in VSNs is constant and cycle-independent. (F) Quantitative RT-PCR for Trpm4 in female VNO during diestrus and metestrus. Bars show the mean copy numbers ± SD from three independent experiments (n = 2/data point), each carried out as triplicates using total RNA of adult B6 females. Copy numbers per ng total RNA are (144 ± 33) at estrus and (77 ± 24) at diestrus ($p < 0.05$). (G) Schematic representation summarizing expression levels of Trpm4 (dark green, high; light green, low) during the different stages of the estrous cycle (color-coded) and the approximate corresponding levels of the ovarian steroid hormones 17ß-estradiol (E2) and progesterone (P4). L: lumen, ns: non-sensory epithelium. Scale bars, 100 μm. (H, I) Quantification (in a.u.) of Trpm4 (H) and Trpc2 immunofluorescence (I) across the estrous cycle. Trpm4 mean fluorescence intensities are significantly increased during proestrus (676 ± 163, n = 5 mice, 22 sections, 3–7 sections/mouse) and estrus (698 ± 105, n = 5 mice, 30 sections, 4–9 sections/mouse) *versus* metestrus (301 ± 93, n = 4 mice, 28 sections, 6–8 sections/mouse) and diestrus (240 ± 85, n = 4 mice, 26 sections, 5–8 sections/mouse). ANOVA One Way: $P < 0.001$; Tukey's *post hoc* test: ** $p < 0.01$, *** $p ≤ 0.001$; ns: 0.9–1.0. (I) Trpc2 mean fluorescence intensities do not significantly differ between estrous cycle stages. For direct comparison to Trpm4, sections of the same mice were analyzed. Mean fluorescence intensity at metestrus (307 ± 135, n = 4 mice, 22 sections, 4–8 sections/mouse), diestrus (365 ± 89, n = 4 mice, 23 sections, 4–8 sections/mouse), proestrus (500 ± 84, n = 5 mice, 29 sections, 4–8 sections/mouse), and estrus (367 ± 102, n = 5 mice, 24 sections, 3–7 sections/mouse). Kruskal-Wallis ANOVA: $P = 0.08$; Mann-Whitney U test: ns $p = 0.06–0.73$. Data are expressed as means ± SD. Individual data points represent the averaged values obtained from a single mouse.

Together, these results reveal that vomeronasal expression of Trpm4 is sexually dimorphic and synchronized to the female reproductive cycle (Fig. 4G). Remarkably, Trpm4 protein expression is upregulated specifically during proestrus and estrus, when female mice are about to ovulate and become sexually active and receptive. These results identify Trpm4 as a channel candidate in the VNO that could serve for the molecular and neural control of sexually-dimorphic cellular and behavioral responses, and for mediating estrous cycle-dependent and

(caption on next page)

Fig. 5. Trpm4 expression in female VSNs is abolished by OVX and restored by systemic 17ß-estradiol (E2) treatment. (A) Schematic timeline of different treatment protocols performed on adult B6 females with OVX at day 8 and hormone implantation at day 21. Vaginal smears were monitored during experiments (see checker boards) with intermission during surgery recovery periods. Following treatment, mice were sacrificed and analyzed for changes in Trpm4-IR (green fluorescence) in coronal VNO sections (B–F). (B) Trpm4-IR in VSNs is diminished following OVX of B6 females ($n = 12$). OVX induces a persistent post-ovulatory state consisting of metestrus and diestrus (see C–F). (C) The checker board (top) represents the daily estrous cycle stage color-coded as metestrus – white, E, diestrus – grey, D, proestrus – rosé, P, and estrus – red, E. After 5 days of cycle monitoring, OVX was performed on day 8, followed by E2 implantation on day 21. E2 implantation causes a persistent estrus stage (red boxes) and restores Trpm4-IR in VSNs of OVX B6 females ($n = 4$). (D) OVX females receiving vehicle implants on day 21 reside in metestrus/diestrus and maintain the low levels of Trpm4-IR of untreated OVX females ($n = 4$). (E) OVX females receiving E2 implants on day 21 followed by a single P4 injection on day 38 show Trpm4-IR in VSNs 6 h ($n = 3$) post-injection. (F) OVX females receiving P4 implants on day 21 instead of E2 show a persistent diestrus phase (grey boxes). P4 implants do not affect the low level of Trpm4-IR in VSNs of OVX females ($n = 4$). L, lumen; ns, non-sensory epithelium. Scale bars, 100 μm. (G) Quantification of Trpm4 immunofluorescence (in a.u.) in VNE for various treatments: OVX (256 ± 55, $n = 3$ mice, 18 sections, 5–7 sections/mouse); OVX-E2 (442 ± 98, $n = 3$ mice, 18 sections, 5–7 sections/mouse); OVX-E2 6 h post P4 treatment (429 ± 18, $n = 3$ mice, 19 sections, 5–8 sections/mouse); OVX-E2 24 h post P4 treatment (400 ± 47, $n = 3$ mice, 20 sections, 5–8 sections/mouse); OVX-P4 (273 ± 15, $n = 3$ mice, 21 sections, 6–7 sections/mouse). ANOVA One Way: $P = 0.004$; Tukey's *post hoc* test: *p < 0.05, ns $p = 0.1$–1. Data are expressed as means $\pm$ SD. Individual data points represent the averaged values from a single mouse.

hormone-regulated vomeronasal signaling.

3.3. Cyclic Trpm4 regulation depends on ovarian sex hormones

Does the cyclic regulation of Trpm4 protein expression in VSNs depend on internal signals that report the estrous state of a female to the VSNs? The ovaries are a key source for endogenous production of the female sex-steroid hormones 17ß-estradiol (E2) and progesterone (P4) (Fig. 4G), and females lacking ovaries fail to produce significant circulating levels of these hormones (Levine, 2015). To determine whether circulating female ovarian hormones may underlie the cyclic regulation of Trpm4 in VSNs, we manipulated endogenous hormone production by bilateral surgical ovariectomy (OVX) and analyzed Trpm4-IR in the VNE. We performed OVX on adult (6–8 weeks) cycling B6 females (Fig. 5). OVX caused cycle arrest in all cases ($n = 30$; Fig. 5A–F) that was accompanied by downregulation of Trpm4 protein expression in the VNE (Fig. 5B). Thus, vomeronasal Trpm4 expression requires key signals from intact ovaries.

In normally cycling females, both E2 and P4 are present at basal levels throughout the cycle but E2 transiently surges during late proestrus whereas P4 displays a first peak during diestrus and a second smaller peak around the time of estrus (Wood et al., 2007; Levine, 2015). To determine which hormones could be responsible for the modulation of vomeronasal Trpm4 expression, we employed OVX mice, replaced single ovarian hormones by subcutaneous reservoir implants, and analyzed both estrous cycle and Trpm4-IR in the VNE (Fig. 5C-F). Hormone implants (see Materials & methods) were designed to maintain physiological levels of circulating E2 at ~60 pg/ml and P4 at ~15 ng/ml, corresponding to pre-ovulatory plasma concentrations (Wood et al., 2007). Prior to OVX, all mice used in these experiments exhibited a normal cycle of 4–5 days ($n = 18$). Each of these mice became acyclic following OVX (Fig. 5C-F). Mice that received E2 treatment switched from OVX-induced acyclicity to a persistent estrus ($n = 4$; Fig. 5C). Importantly, these mice also showed a significant increase in vomeronasal Trpm4-IR (Fig. 5C), whereas vehicle-treated mice did not (Fig. 5D).

Such E2-induced upregulation of Trpm4-IR was not affected by P4 injection performed 6 h or 24 h prior to transcardial perfusion of the mice (Fig. 5E, G). Furthermore, P4 implantation alone shifted the estrous cycle of OVX mice to a persistent diestrus, but did not cause obvious upregulation of vomeronasal Trpm4-IR (Fig. 5F, G). Therefore, systemic E2 treatment – but not P4 treatment – is sufficient to restore vomeronasal Trpm4 expression in OVX mice, suggesting that an E2 surge could be a key signal for the induction of cyclic Trpm4 upregulation in VSNs.

3.4. Aromatase enzyme is required for upregulation of Trpm4 in female VNO

The enzyme cytochrome-P450 aromatase (also known as estrogen

synthase) is required for estradiol biosynthesis from testosterone (Santen et al., 2009). To determine whether endogenous estradiol production through the activity of aromatase mediates Trpm4 upregulation in VSNs, we administered systemically the aromatase inhibitor exemestane (EXE; 6-methylideneandrosta-1,4-diene-3,17-dione) and analyzed Trpm4-IR (Fig. 6A-C, E). Prior to administration of exemestane or vehicle (sesame oil) (5 mg/kg bodyweight), all mice used in these experiments exhibited a normal estrous cycle of 4–5 days ($n = 6$; Fig. 6B, C). We injected exemestane intraperitoneally (5 consecutive injections over 5 days), assayed vaginal cytology in parallel, and found that all mice entered an anestrous state after only two days of treatment. Importantly, this exemestane-induced acyclicity was accompanied by strongly diminished Trpm4-IR in virtually all VSNs (Fig. 6B, E). By contrast, females of the control group treated with vehicle exhibited normal cyclicity and showed abundant Tpm4-IR in VSNs when sacrificed during estrus (Fig. 6C, E). Therefore, endogenous aromatase activity underlying the biosynthesis of estradiol is required for the upregulation of Trpm4 expression in the VNO of female mice *in vivo*.

3.5. Downregulation of vomeronasal Trpm4 expression in pregnant females

Estrous cycles during sexual maturity of female mice can be interrupted by pregnancy, and blood serum levels of sex hormones change accordingly during this phase. We asked whether vomeronasal Trpm4 expression can also be regulated as a result of pregnancy (Fig. 6D, E). We examined Trpm4-IR in pregnant B6 mice at gestational day 19 (G19, $n = 3$), a late stage of the 21 days of pregnancy that is characterized by excessive P4 plasma levels until parturition (Lonstein et al., 2015). Trpm4-IR in the VNO of these mice was strongly reduced compared to the values obtained from a vehicle-injected control mouse in estrus (Ctrl-E) (Fig. 6D, E) indicating that Trpm4 expression is downregulated in the VNO of pregnant female mice. This result is consistent with our findings during the post-ovulatory phase of the estrous cycle (see Fig. 5 and Fig. 6E). It thus appears that abundant vomeronasal Trpm4 expression would not be required in female mice during sexually non-receptive conditions.

4. Discussion

The vomeronasal pathway plays a central role in understanding sex-specific and state-dependent responses to olfactory and pheromonal cues, but the molecular and neural mechanisms that enable such responses are poorly understood. Recent evidence indicated that response variability may already arise, in part, through modulation at the level of the sensory neurons in the periphery (Dey et al., 2015), in addition to central circuits in the brain (Yang and Shah, 2014; Ishii et al., 2017; Li and Dulac, 2018; McKinsey et al., 2018). Here, we have identified a member of the melastatin subfamily of TRP channels, Trpm4, as a second major TRP channel expressed in VSNs besides Trpc2. Trpm4 is
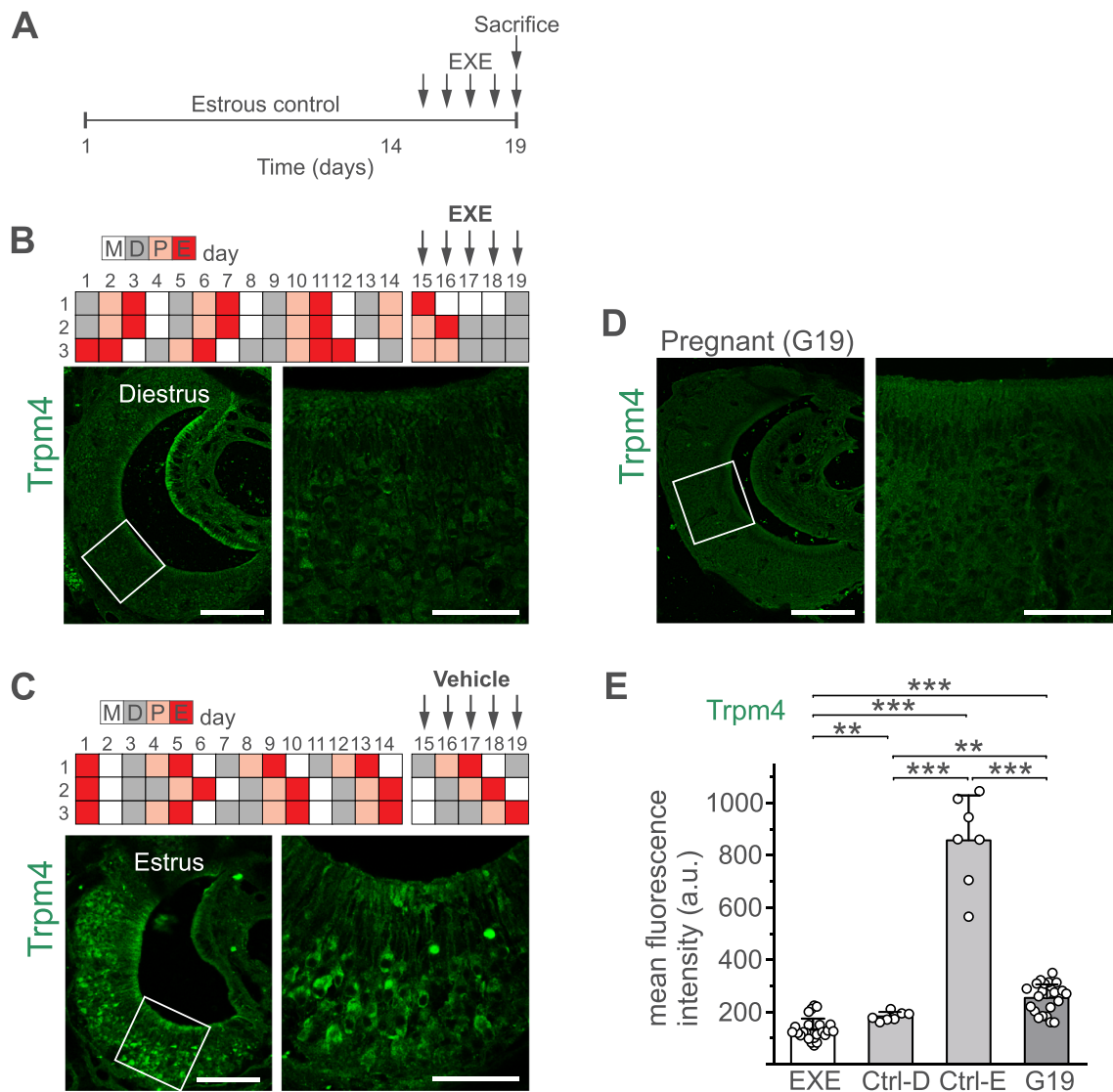
Fig. 6. Vomeronasal Trpm4 expression in female mice depends on endogenous aromatase function and is downregulated during pregnancy. (A) Schematic timeline of adult B6 females treated with the steroidal aromatase inhibitor exemestane (EXE) or vehicle. Females received a single i.p. injection of EXE or vehicle (sesame oil) on five consecutive days (days 15–19). Vaginal smears were analyzed daily throughout the experiment. (B) The checker board (top) represents the daily estrous cycle stage color-coded as metestrus – white, E, diestrus – grey, D, proestrus – rosé, P, and estrus – red, E. Two days after EXE injection, females reside in the post-ovulatory state (metestrus and diestrus). Trpm4-IR (green) in coronal sections of the female VNO following EXE treatment displays diminished Trpm4 staining in VSNs ($n = 3$). (C) Control females ($n = 3$) injected with vehicle (sesame oil) on 5 consecutive days maintain an intact estrous cycle and robust Trpm4 staining of VSNs (green) when sacrificed at estrus. (D) Example of Trpm4-IR (green) in a pregnant B6 mouse at gestational day 19 (G19). L, lumen; ns, non-sensory epithelium; Scale bars: 100 μm. (E) Quantification of Trpm4 immunofluorescence (in a.u.) in VNE for various treatments: EXE-injected (EXE, 134 $\pm$ 43, $n = 4$ mice, 24 sections, 6 sections/mouse); vehicle-treated control in diestrus (Ctrl-D, 183 $\pm$ 17, $n = 1$ mouse, 7 sections); vehicle-treated control in estrus (Ctrl-E, 857 $\pm$ 172, $n = 1$ mouse, 7 sections); G19 (254 $\pm$ 57, $n = 3$ mice, 22 sections, 6−8 sections/mouse). Kruskal-Wallis ANOVA: $P < 0.001$. Mann-Whitney U test: **$p < 0.01$, ***p < 0.001. Data are expressed as means $\pm$ SD. Individual data points represent mean intensities from single VNE sections.

likely to participate in sex-specific, estrous cycle-dependent and sex hormone-regulated functions of the mouse VNO. Its expression differed from that of Trpc2 in two important aspects. First, unlike Trpc2, Trpm4 was not detectable in the microvilli of VSNs, suggesting that Trpm4 does not mediate primary chemoelectrical transduction in VSNs but rather would be ideal for a modulatory function in these neurons. Second, Trpm4 was expressed in a sex-specific manner in VSNs, in contrast to Trpc2. In the VNO of female mice, we found that expression of Trpm4 was synchronized to the female reproductive cycle. This cyclic regulation was governed by ovarian sex hormones as OVX resulted in permanent downregulation of Trpm4 expression, an effect that could be restored by systemic treatment of mice with 17ß-estradiol but not progesterone. Furthermore, cyclic Trpm4 expression required endogenous aromatase activity, and was strongly reduced during a late

stage of pregnancy.

The VNO is heavily vascularized and is readily accessible to circulating steroid hormones (Cherian et al., 2014). Previous work has identified mRNA expression for the estrogen receptors α (*Esr1*) and *Gpr30* in mouse VNO (Cherian et al., 2014; Oboti et al., 2015) and immunohistochemistry identified protein expression for these receptors in isolated mouse VSNs (Cherian et al., 2014). Likewise, mRNA for progesterone receptor membrane components 1 and 2 (*Pgrmc1* and *Pgrmc2*) has been identified in mouse VNO (Oboti et al., 2015) and immunohistochemistry showed Pgrmc1 protein staining with cellular resolution for mouse VSNs (Dey et al., 2015). Thus, the cellular machinery should be in place for mediating the effects of ovarian hormones on VSNs as described here. But while earlier work focused on the rapid, acute effects of 17ß-estradiol on VSN physiology (Cherian et al.,

2014), our current study has identified a critical role for this hormone in the cyclic expression of a specific ion channel in VSNs, Trpm4.

The function of Trpm4 in the nervous system is currently not well understood (Mathar et al., 2014). The *Trpm4* gene encodes one of only two molecularly defined Ca^{2+}-activated cation channels that conduct monovalent but not divalent cations, with *Trpm5* being the second one (Liman, 2007). As we found no evidence for acute Trpm5 expression in VSNs, the Ca^{2+}-activated cation currents that we and others reported previously (Liman, 2003; Spehr et al., 2009) were most likely mediated by Trpm4. Future recordings using $Trpm4^{-/-}$ mice will have to confirm this conjecture. The features of Trpm4 make it well suited to amplify and strengthen sensory responses in VSNs, by increasing the amplitude and/or the duration of VSN receptor potentials. The firing properties of VSNs are ideal to generate prolonged excitatory responses (Ukhanov et al., 2007). Alternatively, strong depolarization of VSNs through Trpm4 could also lead to depolarization block, and thus to diminished excitation. Future experiments will be required to determine the precise role of Trpm4 in the VNO of male and female mice.

It should also be interesting to determine the source of the Ca^{2+} signal and the corresponding second messenger mechanisms underlying Trpm4 activation in intact VSNs. Our results show that Trpm4 protein is present in VSN dendrites and somata but not at the site of primary transduction, the VSN microvilli. Therefore, Ca^{2+} entry through Trpc2 is unlikely to contribute to the activation of Trpm4. Rather, we suggest that Trpm4 activation could depend on Ca^{2+} released from intracellular stores such as the endoplasmic reticulum. In this context, it is interesting to note that the type 3 inositol 1,4,5-trisphopshate receptor (InsP$_3$R3) exhibits a similar subcellular distribution in VSNs as Trpm4 (Chamero et al., 2017). Using gene-targeted mice, we showed previously that InsP$_3$R3 is not required for primary sensory transduction in VSNs (Chamero et al., 2017). This result suggests that InsP$_3$R3 could be part of a second, alternative signaling system. An intriguing hypothesis would be that Trpm4 is gated by InsP$_3$R3-dependent Ca^{2+} release. The recent discovery of photoactivatable DAGs that can be used to stimulate Trpc2 in local subcellular compartments (Leinders-Zufall et al., 2018), together with spatially localized photorelease of InsP$_3$ and/or Ca^{2+} (Chamero et al., 2017), should enable to address these questions in the future.

It should also be rewarding in future experiments to examine the potential role of Trpm4 in sex-specific behaviors such as the assessment of urinary pheromone discrimination, partner preference, and mating behaviors of female mice (Brock et al., 2013). Several other behavioral paradigms in female mice would fulfill the criteria raised by our study for a potential involvement of Trpm4. These include the estrous cycle-dependent avoidance of male odors from the same strain (Yano et al., 2015), which may underlie inbreeding avoidance and kin recognition, and the effect of mating experience on the preference to investigate male urinary pheromones (McCarthy et al., 2018). Trpm4 would be ideal to regulate flexibility and plasticity of vomeronasal responses during pheromonal learning (Brennan and Zufall, 2006; Xu et al., 2016; Marom et al., 2019), for example in the imprinting process of a persistent mate recognition memory in female mice (Kelliher et al., 2006). Trpm4 constitutes an attractive new candidate for addressing these questions genetically. Because of the widespread expression of Trpm4, such experiments will require the generation of mice harboring a conditional deletion of Trpm4 in the olfactory system.

CRediT authorship contribution statement

Eugenia Eckstein: Methodology, Investigation, Formal analysis, Visualization, Writing - original draft, Writing - review & editing.**Martina Pyrski:**Conceptualization, Methodology, Investigation, Formal analysis, Visualization, Writing - original draft, Writing - review & editing.**Silvia Pinto:**Resources, Writing - review & editing.**Marc Freichel:**Resources, Writing - review & editing.**Rudi Vennekens:**Visualization, Resources, Writing - review & editing.**Frank Zufall:**Conceptualization, Methodology, Writing - original draft, Writing - review & editing.

References

Baum, M.J., Bakker, J., 2013. Roles of sex and gonadal steroids in mammalian pheromonal communication. Front. Neuroendocrinol. 34, 268–284.

Blum, T., Moreno-Perez, A., Pyrski, M., Bufe, B., Arifovic, A., Weissgerber, P., Freichel, M., Zufall, F., Leinders-Zufall, T., 2019. Trpc5 deficiency causes hypoprolactinemia and altered function of oscillatory dopamine neurons in the arcuate nucleus. Proc. Natl. Acad. Sci. U. S. A. 116, 15236–15243.

Boillat, M., Challet, L., Rossier, D., Kan, C., Carleton, A., Rodriguez, I., 2015. The vomeronasal system mediates sick conspecific avoidance. Curr. Biol. 25, 251–255.

Brennan, P.A., Zufall, F., 2006. Pheromonal communication in vertebrates. Nature 444, 308–315.

Brock, O., Bakker, J., Baum, M.J., 2013. Assessment of urinary pheromone discrimination, partner preference, and mating behaviors in female mice. Methods Mol. Biol. 1068, 319–329.

Bufe, B., Teuchert, Y., Schmid, A., Pyrski, M., Pérez-Gómez, A., Eisenbeis, J., Timm, T., Ishii, T., Lochnit, G., Bischoff, M., Mombaerts, P., Leinders-Zufall, T., Zufall, F., 2019. Bacterial MgrB peptide activates chemoreceptor Fpr3 in mouse accessory olfactory system and drives avoidance behaviour. Nat. Commun. 10, 4889.

Caligioni, C.S., 2009. Assessing reproductive status/stages in mice. Curr. Protoc. Neurosci. 48, A.4I.1–A.4I.8.

Chamero, P., Marton, T.F., Logan, D.W., Flanagan, K., Cruz, J.R., Saghatelian, A., Cravatt, B.F., Stowers, L., 2007. Identification of protein pheromones that promote aggressive behaviour. Nature 450, 899–902.

Chamero, P., Leinders-Zufall, T., Zufall, F., 2012. From genes to social communication: molecular sensing by the vomeronasal organ. Trends Neurosci. 35, 597–606.

Chamero, P., Weiss, J., Alonso, M.T., Rodríguez-Prados, M., Hisatsune, C., Mikoshiba, K., Leinders-Zufall, T., Zufall, F., 2017. Type 3 inositol 1,4,5-trisphosphate receptor is dispensable for sensory activation of the mammalian vomeronasal organ. Sci. Rep. 7, 10260.

Cherian, S., Wai Lam, Y., McDaniels, I., Struziak, M., Delay, R.J., 2014. Estradiol rapidly modulates odor responses in mouse vomeronasal sensory neurons. Neuroscience 269, 43–58.

Dey, S., Chamero, P., Pru, J.K., Chien, M.S., Ibarra-Soria, X., Spencer, K.R., Logan, D.W., Matsunami, H., Peluso, J.J., Stowers, L., 2015. Cyclic regulation of sensory perception by a female hormone alters behavior. Cell 161, 1334–1344.

Dutta Banik, D., Martin, L.E., Freichel, M., Torregrossa, A.M., Medler, K.F., 2018. TRPM4 and TRPM5 are both required for normal signaling in taste receptor cells. Proc. Natl. Acad. Sci. U. S. A. 115, E772–E781.

Haga, S., Hattori, T., Sato, T., Sato, K., Matsuda, S., Kobayakawa, R., Sakano, H., Yoshihara, Y., Kikusui, T., Touhara, K., 2010. The male mouse pheromone ESP1 enhances female sexual receptive behaviour through a specific vomeronasal receptor. Nature 466, 118–122.

Ishii, K.K., Osakada, T., Mori, H., Miyasaka, N., Yoshihara, Y., Miyamichi, K., Touhara, K., 2017. A labeled-line neural circuit for pheromone-mediated sexual behaviors in mice. Neuron 95, 123–137 e128.

Kelliher, K.R., Spehr, M., Li, X.H., Zufall, F., Leinders-Zufall, T., 2006. Pheromonal recognition memory induced by TRPC2-independent vomeronasal sensing. Eur. J. Neurosci. 23, 3385–3390.

Kusumakshi, S., Voigt, A., Hübner, S., Hermans-Borgmeyer, I., Ortalli, A., Pyrski, M., Dörr, J., Zufall, F., Flockerzi, V., Meyerhof, W., Montmayeur, J.P., Boehm, U., 2015. A binary genetic approach to characterize TRPM5 cells in mice. Chem. Senses 40, 413–425.

Launay, P., Fleig, A., Perraud, A.-L., Scharenberg, A.M., Penner, R., Kinet, J.-P., 2002. TRPM4 is a Ca^{2+}-activated nonselective cation channel mediating cell membrane depolarization. Cell 109, 397–407.

Launay, P., Cheng, H., Srivatsan, S., Penner, R., Fleig, A., Kinet, J.P., 2004. TRPM4

regulates calcium oscillations after T cell activation. Science 306, 1374–1377.

Leinders-Zufall, T., Lane, A.P., Puche, A.C., Ma, W., Novotny, M.V., Shipley, M.T., Zufall, F., 2000. Ultrasensitive pheromone detection by mammalian vomeronasal neurons. Nature 405, 792–796.

Leinders-Zufall, T., Ishii, T., Mombaerts, P., Zufall, F., Boehm, T., 2009. Structural requirements for the activation of vomeronasal sensory neurons by MHC peptides. Nat. Neurosci. 12, 1551–1558.

Leinders-Zufall, T., Storch, U., Bleymehl, K., Mederos, Y., Schnitzler, M., Frank, J.A., Konrad, D.B., Trauner, D., Gudermann, T., Zufall, F., 2018. PhoDAGs enable optical control of diacylglycerol-sensitive transient receptor potential channels. Cell Chem. Biol. 25, 215–223.

Leiva-Salcedo, E., Riquelme, D., Cerda, O., Stutzin, A., 2017. TRPM4 activation by chemically- and oxygen deprivation-induced ischemia and reperfusion triggers neuronal death. Channels (Austin) 11, 624–635.

Levine, J.E., 2015. Neuroendocrine control of the ovarian cycle of the rat. In: Plant, T.M., Zeleznik, A.J. (Eds.), Knobil and Neill's Physiology of Reproduction. Academic Press, pp. 1199–1257.

Leypold, B.G., Yu, C.R., Leinders-Zufall, T., Kim, M.M., Zufall, F., Axel, R., 2002. Altered sexual and social behaviors in trp2 mutant mice. Proc. Natl. Acad. Sci. U. S. A. 99, 6376–6381.

Li, Y., Dulac, C., 2018. Neural coding of sex-specific social information in the mouse brain. Curr. Opin. Neurobiol. 53, 120–130.

Liberles, S.D., 2014. Mammalian pheromones. Annu. Rev. Physiol. 76, 151–175.

Liman, E.R., 2003. Regulation by voltage and adenine nucleotides of a Ca^{2+}-activated cation channel from hamster vomeronasal sensory neurons. J. Physiol. 548, 777–787.

Liman, E.R., 2007. The Ca^{2+}-activated TRP channels: TRPM4 and TRPM5. In: Liedtke, W.B., Heller, S. (Eds.), TRP Ion Channel Function in Sensory Transduction and Cellular Signaling Cascades. Boca Raton, FL.

Liman, E.R., Corey, D.P., Dulac, C., 1999. TRP2: a candidate transduction channel for mammalian pheromone sensory signaling. Proc. Natl. Acad. Sci. U. S. A. 96, 5791–5796.

Lonstein, J.S., Pereira, M., Morrell, J.I., Marler, C.A., 2015. Parenting behavior. In: Plant, T.M., Zeleznik, A.J. (Eds.), Knobil and Neill's Physiology of Reproduction. Academic Press, pp. 2371–2437.

Lucas, P., Ukhanov, K., Leinders-Zufall, T., Zufall, F., 2003. A diacylglycerol-gated cation channel in vomeronasal neuron dendrites is impaired in *TRPC2* mutant mice: mechanism of pheromone transduction. Neuron 40, 551–561.

Marom, K., Horesh, N., Abu-Snieneh, A., Dafni, A., Paul, R., Fleck, D., Spehr, M., Ben-Shaul, Y., 2019. The vomeronasal system can learn novel stimulus response pairings. Cell Rep. 27, 676–684.e676.

Mathar, I., Jacobs, G., Kecskes, M., Menigoz, A., Philippaert, K., Vennekens, R., 2014. TRPM4. In: Nilius, B., Flockerzi, V. (Eds.), Mammalian Transient Receptor Potential (TRP) Cation Channels. Springer, Heidelberg New York Dordrecht London, pp. 461–487.

McCarthy, E.A., Naik, A.S., Coyne, A.F., Cherry, J.A., Baum, M.J., 2018. Effect of ovarian hormones and mating experience on the preference of female mice to investigate male urinary pheromones. Chem. Senses 43, 97–104.

McKinsey, G.L., Ahmed, O.M., Shah, N.M., 2018. Neural control of sexually dimorphic social behaviors. Curr. Opin. Physiol. 6, 89–95.

Mohrhardt, J., Nagel, M., Fleck, D., Ben-Shaul, Y., Spehr, M., 2018. Signal detection and coding in the accessory olfactory system. Chem. Senses 43, 667–695.

Murakami, M., Xu, F., Miyoshi, I., Sato, E., Ono, K., Iijima, T., 2003. Identification and characterization of the murine TRPM4 channel. Biochem. Biophys. Res. Commun. 307, 522–528.

Nilius, B., Prenen, J., Droogmans, G., Voets, T., Vennekens, R., Freichel, M., Wissenbach, U., Flockerzi, V., 2003. Voltage dependence of the Ca^{2+}-activated cation channel TRPM4. J. Biol. Chem. 278, 30813–30820.

Oboti, L., Pérez-Gómez, A., Keller, M., Jacobi, E., Birnbaumer, L., Leinders-Zufall, T., Zufall, F., Chamero, P., 2014. A wide range of pheromone-stimulated sexual and reproductive behaviors in female mice depend on G protein Gαo. BMC Biol. 12, 31.

Oboti, L., Ibarra-Soria, X., Perez-Gomez, A., Schmid, A., Pyrski, M., Paschek, N., Kircher, S., Logan, D.W., Leinders-Zufall, T., Zufall, F., Chamero, P., 2015. Pregnancy and estrogen enhance neural progenitor-cell proliferation in the vomeronasal sensory epithelium. BMC Biol. 13, 104.

Ogura, T., Krosnowski, K., Zhang, L., Bekkerman, M., Lin, W., 2010. Chemoreception regulates chemical access to mouse vomeronasal organ: role of solitary chemosensory cells. PLoS One 5, e11924.

Papes, F., Logan, D.W., Stowers, L., 2010. The vomeronasal organ mediates interspecies defensive behaviors through detection of protein pheromone homologs. Cell 141, 692–703.

Pérez-Gómez, A., Bleymehl, K., Stein, B., Pyrski, M., Birnbaumer, L., Munger, S.D., Leinders-Zufall, T., Zufall, F., Chamero, P., 2015. Innate predator odor aversion driven by parallel olfactory subsystems that converge in the ventromedial hypothalamus. Curr. Biol. 25, 1340–1346.

Potter, S.M., Zheng, C., Koos, D.S., Feinstein, P., Fraser, S.E., Mombaerts, P., 2001. Structure and emergence of specific olfactory glomeruli in the mouse. J. Neurosci. 21, 9713–9723.

Pyrski, M., Eckstein, E., Schmid, A., Bufe, B., Weiss, J., Chubanov, V., Boehm, U., Zufall, F., 2017. Trpm5 expression in the olfactory epithelium. Mol. Cell. Neurosci. 80, 75–88.

Santen, R.J., Brodie, H., Simpson, E.R., Siiteri, P.K., Brodie, A., 2009. History of aromatase: saga of an important biological mediator and therapeutic target. Endocr. Rev. 30, 343–375.

Schattling, B., Steinbach, K., Thies, E., Kruse, M., Menigoz, A., Ufer, F., Flockerzi, V., Bruck, W., Pongs, O., Vennekens, R., Kneussel, M., Freichel, M., Merkler, D., Friese, M.A., 2012. TRPM4 cation channel mediates axonal and neuronal degeneration in experimental autoimmune encephalomyelitis and multiple sclerosis. Nat. Med. 18, 1805–1811.

Simard, J.M., Gerzanich, V., 2018. TRPM4 and the emperor. Channels (Austin) 12, 174–175.

Simard, J.M., Woo, S.K., Gerzanich, V., 2012. Transient receptor potential melastatin 4 and cell death. Pflügers Arch 464, 573–582.

Spehr, J., Hagendorf, S., Weiss, J., Spehr, M., Leinders-Zufall, T., Zufall, F., 2009. Ca^{2+}-calmodulin feedback mediates sensory adaptation and inhibits pheromone-sensitive ion channels in the vomeronasal organ. J. Neurosci. 29, 2125–2135.

Stowers, L., Liberles, S.D., 2016. State-dependent responses to sex pheromones in mouse. Curr. Opin. Neurobiol. 38, 74–79.

Stowers, L., Holy, T.E., Meister, M., Dulac, C., Koentges, G., 2002. Loss of sex discrimination and male-male aggression in mice deficient for TRP2. Science 295, 1493–1500.

Tirindelli, R., Dibattista, M., Pifferi, S., Menini, A., 2009. From pheromones to behavior. Physiol. Rev. 89, 921–956.

Tizzano, M., Cristofoletti, M., Sbarbati, A., Finger, T.E., 2011. Expression of taste receptors in solitary chemosensory cells of rodent airways. BMC Pulm. Med. 11, 3.

Trouillet, A.-C., Keller, M., Weiss, J., Leinders-Zufall, T., Birnbaumer, L., Zufall, F., Chamero, P., 2019. Central role of G protein Gαi2 and Gαi2$^+$ vomeronasal neurons in balancing territorial and infant-directed aggression of male mice. Proc. Natl. Acad. Sci. U. S. A. 116, 5135–5143.

Ukhanov, K., Leinders-Zufall, T., Zufall, F., 2007. Patch-clamp analysis of gene-targeted vomeronasal neurons expressing a defined V1r or V2r receptor: ionic mechanisms underlying persistent firing. J. Neurophysiol. 98, 2357–2369.

Vennekens, R., Olausson, J., Meissner, M., Bloch, W., Mathar, I., Philipp, S.E., Schmitz, F., Weissgerber, P., Nilius, B., Flockerzi, V., Freichel, M., 2007. Increased IgE-dependent mast cell activation and anaphylactic responses in mice lacking the calcium-activated nonselective cation channel TRPM4. Nat. Immunol. 8, 312–320.

Wen, S., Götze, I.N., Mai, O., Schauer, C., Leinders-Zufall, T., Boehm, U., 2011. Genetic identification of GnRH receptor neurons: a new model for studying neural circuits underlying reproductive physiology in the mouse brain. Endocrinology 152, 1515–1526.

Wood, G.A., Fata, J.E., Watson, K.L., Khokha, R., 2007. Circulating hormones and estrous stage predict cellular and stromal remodeling in murine uterus. Reproduction 133, 1035–1044.

Xu, P.S., Lee, D., Holy, T.E., 2016. Experience-dependent plasticity drives individual differences in pheromone-sensing neurons. Neuron 91, 878–892.

Yang, C.F., Shah, N.M., 2014. Representing sex in the brain, one module at a time. Neuron 82, 261–278.

Yang, T., Shah, N.M., 2016. Molecular and neural control of sexually dimorphic social behaviors. Curr. Opin. Neurobiol. 38, 89–95.

Yano, S., Sakamoto, K.Q., Habara, Y., 2015. Female mice avoid male odor from the same strain via the vomeronasal system in an estrogen-dependent manner. Chem. Senses 40, 641–648.

Zufall, F., 2014. TRPs in olfaction. In: Nilius, B., Flockerzi, V. (Eds.), Mammalian Transient Receptor Potential (TRP) Cation Channels. Springer-Verlag, Berlin Heidelberg, pp. 917–933.